

Research Article

Removal of Cr(VI) ion from aqueous solution using jute stick lignin and application of machine learning approach to determine optimal parameters

Nadim Ahmed^a, Abdullah Al Rakib^b, Md. Shahabuddin^b, Mohammad Shahid Ullah^c, Md. Nurnobi Rashed^d, Md. Jalil Miah^{e,*}

^aDepartment of Electrical and Electronic Engineering, Islamic University of Technology, Board Bazar, Gazipur, 1704, Bangladesh

^bDepartment of Chemistry, Dhaka University of Engineering & Technology, Gazipur, Gazipur-1707, Bangladesh

^cDepartment of Arts and Sciences, Ahsanullah University of Science and Technology, Dhaka, 1208, Bangladesh

^dDepartment of Chemistry, Bangladesh University of Engineering and Technology, Dhaka, 1000, Bangladesh

^eDepartment of Natural Sciences, Islamic University of Technology, Board Bazar, Gazipur, 1704, Bangladesh

ARTICLE INFO

Keywords:
Adsorption
Chromium
KNN
Lignin
XGBoost

ABSTRACT

Adsorption of chromium ions from aqueous solution onto lignin was optimized and modeled under a wide variety of physicochemical factors using machine learning (ML) algorithms. Adsorbent lignin was extracted from jute stick, characterized by different analytical methods, and used for the removal of Cr(VI) ion from aqueous solution. The effects of initial concentration, dosages, pH, duration of adsorption, and temperatures on the adsorption process were studied in batch experiments to determine the optimal parameters. Lignin demonstrated a maximum adsorption capacity of 97.06 mg g⁻¹ at pH 2, and a lignin dose of 50 mg L⁻¹. Various isotherm and kinetic models were used to interpret the data, and the findings established that the adsorption process is best described by the Langmuir isotherm (R² = 0.987), and pseudo-first-order kinetic model (R² = 0.978). The experiment was used to train ML algorithms to find out the relative importance of the influencing factors and to identify the most significant parameter governing Cr(VI) adsorption onto lignin. Four ML models, i.e., random forest (RF), extreme gradient boosting (XGBoost), artificial neural networks (ANNs), and k-nearest neighbors (KNNs), were employed for predictive analysis, determining optimal adsorption conditions, and identifying the most influential parameter. Among the four ML models, KNN and XGBoost provided the highest accuracy for optimizing Cr(VI) adsorption onto lignin. The ML results consistently identified adsorbent dosage as the most promising parameter, followed by temperature and initial concentration.

1. Introduction

The contamination of soil and aquatic habitats by heavy metals represents a significant planetary threat resulting from their persistent characteristics, resistance to natural breakdown, and ability to accumulate in biological organisms (Han *et al.*, 2007). Many heavy metals are frequently utilized in a wide variety of industrial sectors owing to their ability to resist corrosion. Various kinds of industrial goods, e.g., leather processing materials, ceramics, anti-corrosion materials, dyes, pigments, etc., usually utilize chromium metals and related chemicals. Most of the time, chromium-containing waste materials are drained into the aqueous environment or soil through industrial effluents (Li *et al.*, 2020). Chromium is a mutation-triggering, lethal, tumor, and cancer-promoting material; thus, the existence of chromium in an aqueous environment or open surface might pose a severe hazard to the ecosystem as well as human and animal life (Sun *et al.*, 2015). Lignin was chosen as the target adsorbent. Trivalent [Cr(III)] and hexavalent [Cr(VI)] chromium ions are the most stable forms that exist in aqueous solution (Troiano *et al.*, 2013). While Cr(III) plays a role as a trace nutrient in humans, Cr(VI) is highly toxic. Owing to its structural similarity to sulfate and phosphate anions, Cr(VI)

readily enters cells through non-specific anion transporters, leading to oxidative stress, DNA damage, and cellular dysfunction (Nickens *et al.*, 2010). Several research studies have revealed that prolonged exposure to Cr(VI) has been linked to lung cancer, kidney damage, and other life-threatening health disorders (DesMarias and Costa, 2019; Pereira *et al.*, 2021).

To mitigate the contamination caused by metals, various stringent rules and regulations need to be implemented to develop effective methodologies for minimizing the release of toxic metal ions within permissible discharge limits. In this respect, a variety of physical and chemical approaches, such as precipitation, filtration, ion exchange, and electrochemical techniques, have been applied to eradicate toxic metals from industrial waste (Singh and Gupta, 2016). Despite their widespread use, these techniques are often limited by high operating costs, the generation of secondary pollutants, and reduced effectiveness at trace concentrations. Thus, to remove metals from wastewater, a treatment method with the qualities of robustness, high efficiency, and cost-effectiveness will be anticipated. In contrast, adsorption is widely acknowledged as a highly effective, handy, and environmentally sustainable technique to eradicate chromium metal from wastewater (Pereira *et al.*, 2021). Numerous agricultural and industrial by-

*Corresponding author:

E-mail address: jalil@iut-dhaka.edu (Md. J Miah)

Received: 02 September, 2025 Accepted: 26 November, 2025 Epub Ahead of Print: 23 February, 2026 Published: 17 March, 2026

DOI: 10.25259/JKSUS_1395_2025

products, such as waste tea, rice hull, shrimp shell, fish scale and bones, sawdust, coconut shell, and lignin, have been explored as inexpensive adsorbents with encouraging results in heavy metal remediation (Afzaal et al., 2022; Othmani et al., 2022; Prabu et al., 2022). Recently, lignin has garnered significant attention for its potential to effectively remove lethal metal ions from aqueous solutions. This interest stems from its abundant availability, convenient extraction process, rapid biodegradability, and possession of a substantial number of active adsorptive sites within its molecular structure. This interest stems from its abundant availability, convenient extraction method, rapid ability to biodegrade, and possession of a substantial number of adsorptive sites within its molecular structure. For these reasons, lignin was chosen as the target adsorbent in this research. In most of the reports, the study involves the preparation of adsorbents at optimal pyrolysis temperatures, evaluating the adsorbent's performance for removing contaminants under different experimental conditions, such as dose, concentration, pH, etc., and then studying adsorption isotherms, kinetics, and mechanisms. The contribution of each variable, like pH, dose, concentration, and temperature, to the accumulated adsorption efficiency is hardly studied. In this respect, to better understand the mutual interaction of different variables on adsorption performance and to determine suitable experimental conditions for high-performance adsorption, it is crucial to adopt different techniques/approaches.

In recent years, the emergence of ML has ushered in transformative changes across multiple disciplines, fundamentally altering our approach to solving complex problems. Its appeal lies in its ability to effectively manage extensive data-driven complexities, high-speed computation, and self-learning capability. These factors contribute to a substantial reduction in the necessary material resources, time, and human workforce for conducting experiments and research. ML predominantly implements modeling and prediction of complex, nonlinear mathematical relationships between independent and dependent variables, allowing it to address a wide range of engineering problems. As a consequence, the field of chemical engineering is experiencing significant growth in the utilization of ML to overcome operational difficulties and environmental issues (Li et al., 2022; Taoufik et al., 2022). ML algorithms are employed to improve computational chemistry, the synthesis of novel materials, and methods for removing environmental pollutants (Dobbelaere et al., 2021).

Recently, ML techniques were widely utilized to predict the performance and efficiency of adsorption processes. Zhu et al. (Zhu et al., 2019) used random forest (RF) and artificial neural network (ANN) for predicting metal sorption onto biochar, with RF showing better accuracy and predictive performance. In another study (Zhu et al., 2021), they utilized gradient boosting trees, ANN, and RF models to precisely predict the removal of antibiotics such as tetracycline (TC) and sulfamethoxazole (SMX) by biochars (2021). Zhang et al. (Zhang et al., 2023) employed several ML techniques, namely AdaBoost, LGBost, and extreme gradient boosting (XGBoost), to establish predictive models for adsorptive removal of As(III) and As(V) onto biochar. The models were constructed utilizing data obtained from relevant literature sources about the adsorption of arsenic (As) onto biochar. Wu et al. (Wu et al., 2023) assessed phosphate adsorption in terms of textural properties and metal compositions using three separate tree-based ML algorithms, namely RF, decision trees (DTs), and XGBoost. Zafar et al. (Zafar et al., 2022) developed ANN and adaptive neuro-fuzzy inference system (ANFIS) models to predict chromium removal in a modified maghemite nanoparticles adsorption system. However, there is a lack of ML-aided predictive models for the prediction of chromium adsorption by lignin. To investigate the underlying dependent relationships between chromium adsorption performances and lignin material properties and adsorption conditions, a data-driven framework is required.

To bridge this existing knowledge gap, this study sought to evaluate the adsorption potential of lignin for removing chromium ions (Cr(VI)) from aqueous solutions. This work integrates both experimental analyses and a data-driven approach supported by ML techniques. In this study, Lignin was extracted from jute sticks, characterized, and subsequently employed to eliminate Cr(VI) ions from water. The experiment data were employed to develop four ML algorithms, such as RF, XGBoost, K-Nearest Neighbor (KNN), and ANN, for predicting the adsorption behavior of lignin towards chromium ions. Understanding the adsorption

behavior of chromium ions onto lignin, and the influence of various variables like initial chromium ion concentration, pH, adsorbent dosage, time of adsorption, and temperature on the adsorption performance is a challenging task. However, ML algorithms could be utilized to provide us with such insights. Hence, this report particularly sought to (i) establish generalized models to predict the adsorption efficiency of chromium ions on lignin surface, based on set of variables derived from material characteristics and adsorption experiment settings; (ii) perform a competitive investigation of the developed ML models to identify the most effective predictive method that can efficiently be applied for finding the optimal experimental conditions; (iii) evaluate the relative importance and influence of individual parameters on the adsorption and find out the most significant variables; (iv) elucidate the complex interrelationships among these variables on the adsorption efficiency.

Overall, this study filled a gap in existing research by developing a generalized ML model for predicting chromium adsorption onto lignin surface. It delivers an exhaustive elucidation of chromium removal via lignin, emphasizing the critical influence of experimental parameters and delineating the optimal conditions for maximal adsorption efficacy.

2. Materials and Methods

2.1 Preparation of adsorbent

The preparation of the adsorbent method for the characterization of adsorbent, adsorption experimental procedures, and batch experiments for the study of adsorption kinetics and isotherms have been described in the [supplementary information](#).

2.2 Data preprocessing for ML algorithms

From the experiment of Cr(VI) adsorption onto Lignin, 145 data points were extracted and used for ML models. The parameters considered as input data for the models were (i) initial concentration of Cr(VI); (ii) adsorbent dosage; (iii) contact time; (iv) solution pH; and (v) temperature. At the same time, the percentage removal of Cr(VI) was selected as the output of the models. Linear dependence between any two input parameters or between any input parameter and the targeted output parameter (i.e., percentage removal of Cr(VI)) was inspected by Pearson's correlation coefficient (PCC) (Benesty et al., 2009), given by Eq. (1).

$$r_{xy} = \frac{\sum_{i=1}^n (x_i - \bar{x}) \sum_{i=1}^n (y_i - \bar{y})}{\sqrt{\sum_{i=1}^n (x_i - \bar{x})^2} \sqrt{\sum_{i=1}^n (y_i - \bar{y})^2}} \quad (1)$$

Where, r_{xy} is the PCC value between any two parameters x and y . \bar{x} or \bar{y} are the mean value of the variable x or y . PCC ranges between 1 and -1 . $r_{xy} = 1$ denotes a strong linear dependence between the variables, while $r_{xy} = -1$ indicates a high negative correlation. $r_{xy} = 0$ suggests there is no correlation between the variables.

Prior to training the ML models, the data of input variables undergo normalization using the Z-score standardization approach as described in Eq. (2).

$$x_i^* = \frac{(x_i - \mu)}{\sigma} \quad (2)$$

Where, x_i^* indicates the normalized value of the original variable x_i . μ and σ are the mean value and the standard deviation of x_i , respectively. Some data points were observed that significantly deviate from the mean value of the dataset. Generally, these data points can exhibit unusual behavior or extreme observations. They were identified and eliminated using the Z-score. The data points with a z-score ≥ 3 or ≤ -3 are considered extreme and are flagged for removal.

2.3 ML models

For predicting Cr(IV) uptake by lignin under different conditions in terms of material characteristics and adsorption conditions, four supervised ML algorithms, i.e., RF, XGB, ANN, and KNN, were selected.

RF represents an ensemble methodology, integrating several DTs to enhance accuracy in prediction and reduce overfitting (Breiman, 2001). RF produces a collection of DTs, with each tree trained on a distinct, randomly drawn portion of the original dataset and a randomly sampled offset of input features. These trees independently train, and their predictions aggregate through averaging to yield the final output. By leveraging the diverse perspectives of multiple trees, RF effectively reduces overfitting and enhances prediction accuracy.

XGBoost is an advanced ensemble learning method based on the gradient boosting framework (Chen and Guestrin, 2016). This framework sequentially constructs DTs in a boosting approach, where each tree actively corrects errors from preceding trees by assigning greater weights to mispredicted samples. Gradient descent optimization techniques are utilized to minimize its loss function. XGBoost incorporates regularization techniques into the objective function, allowing it to control the complexity of individual trees and prevent overfitting. It is designed to be highly parallelizable, making it more efficient for multi-core processors (Mamudur and Kattamuri, 2020). It can build trees in parallel, which significantly speeds up training compared to traditional Gradient Boosting, which builds trees sequentially.

ANN draws inspiration from biological neural systems (Jain et al., 1996). ANNs are composed of multiple interconnected layers of artificial neurons, which include input, hidden, and output layers. Each connection between neurons has a weight that adjusts during training. Neurons apply activation functions (i.e., Sigmoid, ReLU, Leaky ReLU, Tanh, etc.) to their weighted inputs, enabling complex computations (Apicella et al., 2021). The process initiates with feedforward propagation, where input data flows through the network, producing an output. A loss function measures the prediction error compared to the actual target. Backpropagation adjusts weights by propagating error backward through the network, using techniques like gradient descent. This iterative process continues until the network's performance is satisfactory. In our study, ANN consisted of an input layer with five independent variables according to the experimental data, followed by three hidden layers comprising 50, 350, and 50 neurons, and lastly, an output layer that predicted removal efficiency.

The KNN method forecasts outcomes for new data points using the K most proximate neighbors in the dataset. (Kramer, 2013). The process involves selecting an optimal K, computing distances between the new data point and all training data using metrics such as Euclidean or Manhattan distance, and choosing the K closest neighbors. Finally, the prediction is computed from the average of the KNN target output.

To achieve accurate predictions and ensure robust generalization capabilities, it is essential to carefully tune the hyperparameters for each ML model. Hyperparameters, parameters fixed prior to training and not learned from training data (Probst et al., 2019), were optimized using grid search (Bergstra and Bengio, 2012) combined with 5-fold cross-validation (Refaeilzadeh et al., 2009). This method systematically explores a predefined hyperparameter grid by randomly splitting the dataset into five folds. For each hyperparameter set, models are trained on four folds and evaluated(test) on the remaining fold. Repeating this process five times, the average performance identifies the best hyperparameters, ensuring models generalize well and avoid overfitting.

2.4 Performance evaluation

The performance of ML algorithms in this research was measured using four different metrics i.e., mean absolute error (MAE), mean squared error (MSE), root mean square error (RMSE), and coefficient of determination (R^2). MAE, MSE, RMSE, and R^2 can be expressed mathematically using Eqs. (3-6), respectively.

$$MAE = \frac{1}{N} \sum_{i=1}^N |y_i - \hat{y}_i| \quad (3)$$

$$MSE = \frac{1}{N} \sum_{i=1}^N (y_i - \hat{y}_i)^2 \quad (4)$$

$$RMSE = \sqrt{\frac{\sum_{i=1}^N (y_i - \hat{y}_i)^2}{N}} \quad (5)$$

$$R^2 = 1 - \frac{\sum_{i=1}^N (y_i - \hat{y}_i)^2}{\sum_{i=1}^N (y_i - \bar{y})^2} \quad (6)$$

Where, y_i and \hat{y}_i are actual and predicted values of the target parameter, respectively. \bar{y} denotes the average of all instances of the target variable in the dataset. N denotes the number of instances. A ML model's predictive performance is considered better when it exhibits a higher R^2 value and lower values for MAE, MSE, and RMSE (N. Moriasi et al., 2007; Shahmansouri et al., 2019).

2.5 Feature importance and partial dependence

Achieving optimal Cr(VI) adsorption by lignin requires a thorough analysis of each input parameter's impact on the adsorption process. This analysis reveals optimal material characteristics and experimental conditions. To quantify each parameter's contribution to removal efficiency, feature importance analysis was performed. Among four ML models, XGBoost and KNN were chosen due to their superior performance. Permutation feature importance (Altmann et al., 2010) was used to calculate feature importance for these models. Permutation feature importance measures the effect on the model's prediction error when the values of a single feature are permuted (Molnar et al., 2020). By disrupting the relationship between the input data and the target feature, this approach indicates the extent to which the algorithm relies on the feature. Although permutation importance identifies the individual contribution of features to overall prediction, it does not reveal how these variables affect adsorption efficiency. To address this, partial dependence plots (PDPs) were applied, illustrating the effect of one or two features on adsorption efficiency in the selected models (Friedman, 2001). Results from both permutation importance and PDP analyses have been detailed in the results section, providing comprehensive insight into the roles of individual input parameters in optimizing Cr(VI) adsorption by lignin.

3. Results and Discussion

3.1 Characterization of the adsorbent

To characterize the jute stick lignin, fourier transform infrared (FTIR) data were recorded over 400–4000 cm^{-1} . A broad peak arises in the wavelength range of 2800–3800 cm^{-1} (Fig. 1), which can be assigned as the stretching vibration of hydroxyl (–OH) groups of lignin. The bands observed at 1669 cm^{-1} , 1631 cm^{-1} , and 1459 cm^{-1} might be due to aromatic skeletal vibration of lignin (Choudhary et al., 2020; Keiluweit et al., 2010). The band at 1050 cm^{-1} is attributed to C–O stretching vibrations of alcohol groups or in-plane C–H aromatic deformations. The band at 685 cm^{-1} describes out-of-plane C–H stretching of aromatic skeletal, while the peak at 560 cm^{-1} is assigned to the out-of-plane bending vibration of O–H groups. The FTIR spectrum of lignin exhibited analogous absorption peaks, with shifting or reduced intensities in several bands, stipulating the uptake of chromium ions due to the adsorption of Cr(VI) onto the lignin surface. After adsorption of Cr(VI), a fresh peak appeared at 2945 cm^{-1} due to C–H stretching of $-\text{CH}_2$ groups, while additional peaks at 1243 cm^{-1} and 1103 cm^{-1} might be assigned to C–H stretching of the tertiary alcoholic groups (Papaevangelou et al., 2023). The experimental FTIR data for the jute sticks lignin are well consistent with the recently published literature on lignin derived from agricultural waste (Md Salim et al., 2021; Nguyen-Thi et al., 2024).

Scanning Electron Microscopy (SEM) images were used to observe the structural morphology of lignin, see Fig. 2. The SEM images reveal

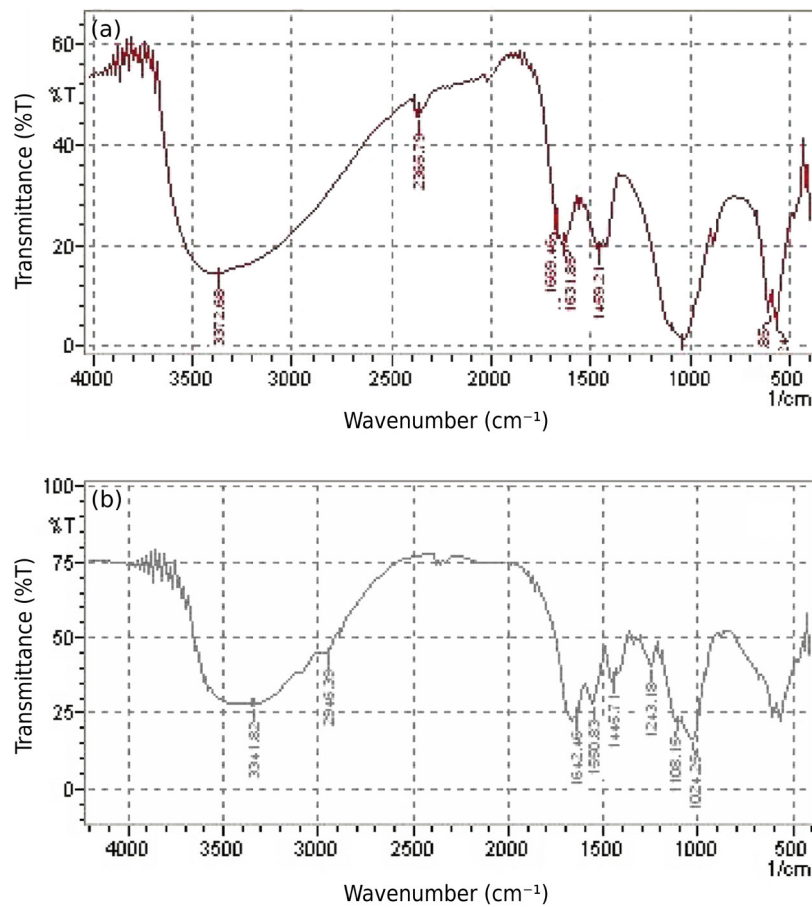


Fig. 1. FTIR spectrum of lignin (a) before adsorption, (b) after Adsorption of Cr(VI) from aqueous solution by using jute stick lignin.

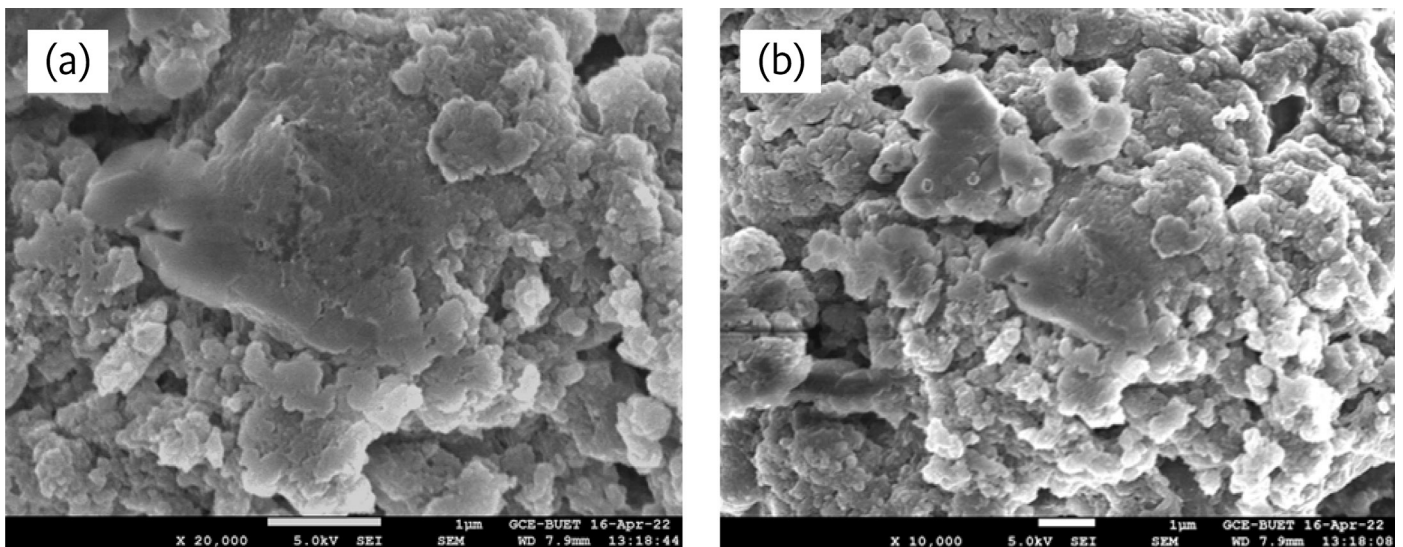


Fig. 2. SEM image of lignin (a) before adsorption, (b) after adsorption of Cr(VI) ions.

lignin consists of a 3D layered arrangement of sheets of varying sizes and shapes. The lignin sheets display a very flat and smooth surface with a porous microstructure. SEM images of lignin after the adsorption of Cr(VI) also demonstrate a 3D layer arrangement of sheets, but surface roughness is more pronounced compared to the lignin surface before the adsorption of chromium due to the uptake of Cr(VI) onto the surface of lignin.

Fig. 3(a) shows the UV-visible spectra of lignin prepared from jute sticks. The spectra showed a wide adsorption peak from 250–300 nm

and a shoulder peak at 300–350 nm. The characteristic absorption band between 250–300 nm ascribes the $\pi \rightarrow \pi^*$ transition of unsaturated benzene rings and the aromatic hydroxy groups of lignin. The associated shoulder band observed at 300–350 nm is assigned to the $n \rightarrow \pi^*$ transition of α - β unsaturated and α -carbonyl functionalities of lignin molecules (Mohamad Ibrahim et al., 2011). These characteristic and prominent absorption peaks indicate that lignin is structurally composed of different aromatic rings and alcohol groups such as synapyl alcohol, p-coumaryl alcohol, and coniferyl alcohol (Kumar and

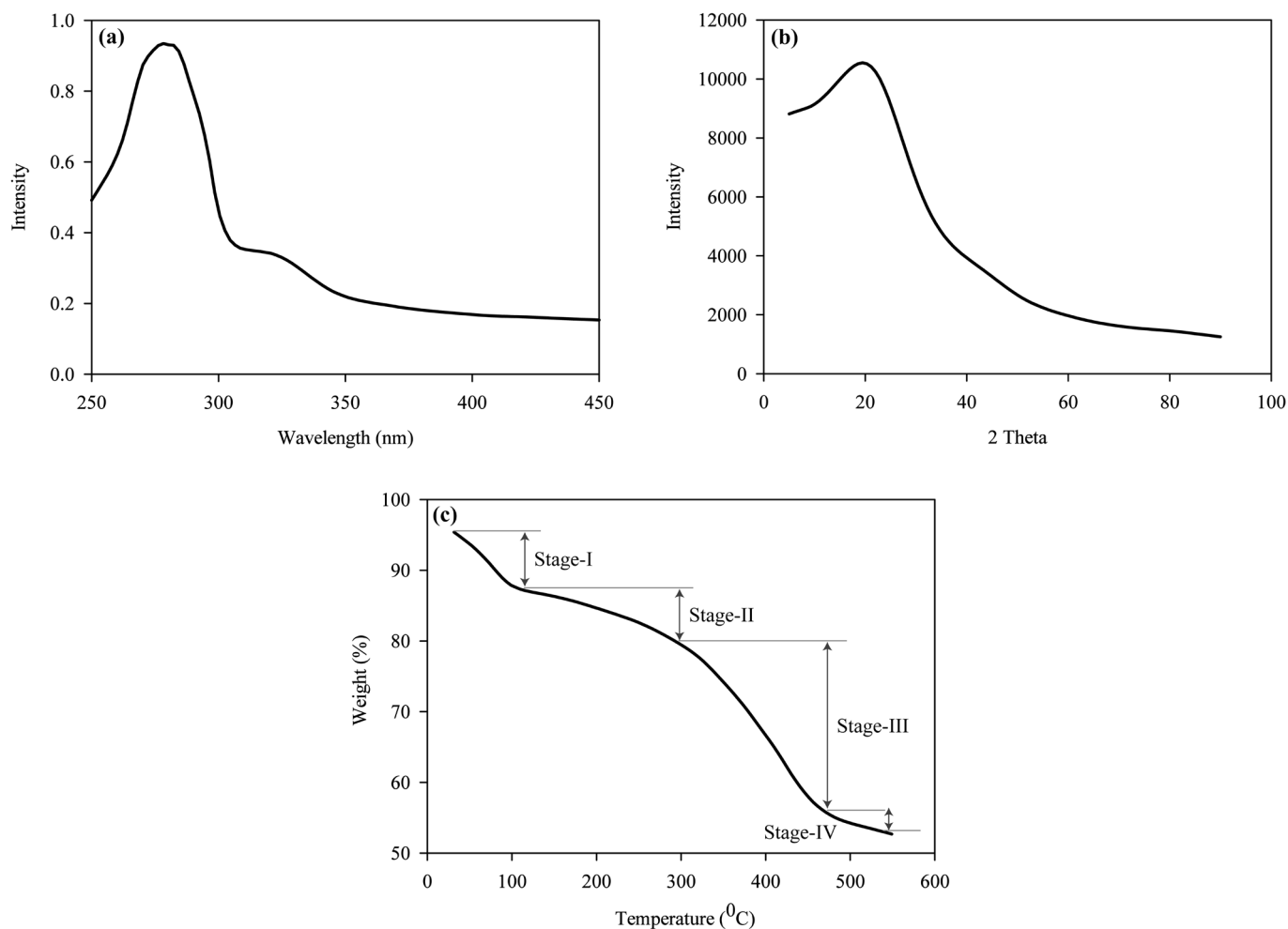


Fig. 3. (a) UV-visible spectra, (b) X-ray diffraction pattern, and (c) TGA thermogram of lignin.

Dwivedi, 2021). To further characterize lignin, powder X-ray diffraction was carried out, and Fig. 3(b) demonstrates the X-ray diffractogram of lignin. A broad, intense reflection band is observed over a wide 2θ range of 20° – 30° . This suggests that the lignin surface is amorphous in nature, where 2D graphene sheets are packed together into small domains of carbon nanosheets. Furthermore, the maximum values of 2θ arise at 20.42° ; this stipulates that type-I cellulose predominantly forms the lignin structure (Dutta et al., 2022).

Fig. 3(c) represents the thermogravimetric analysis (TGA) of jute stick lignin. The thermogram shows that the degradation of lignin occurred in four different stages within temperature ranges of 50 – 600°C . Stage-I (50 – 130°C) is the volatilization region; water and moisture content evaporate and resulting in about a 10% weight loss of lignin. Stage-II (130 – 290°C) is less steep than stage-I; the different polymeric binders, such as hemicellulose content, degrade slowly over this region. In stage-III (300 – 480°C), decomposition of lignin occurred quite harshly in this area due to the complex linkages between fundamental structural molecules like phenolic, carbonyl, and benzylic hydroxyl groups and the initiation of carbonization in lignin molecules (Nguyen-Thi et al., 2024). In stage-IV ($>480^\circ\text{C}$), charcoal or coke carbon is formed due to extensive cross-linking and the formation of a highly dense aromatic structure.

3.2 Comparison of different ML models

In this study, four ML models (RF, XGBoost, ANN, and KNN) were used to predict Cr(VI) adsorption by lignin, utilizing the input parameters outlined in the data collection section. During model training, hyperparameter tuning was accomplished using a grid search technique and five-fold cross-validation. The hyperparameters of the

four models were optimized to get superlative predictive performance. Table S2 of the Supplementary information lists the hyperparameters and their tuned values for all ML models. After the development of the ML models and the optimization of their hyperparameters, an evaluation was conducted to assess their prediction accuracy on the dataset. The joint scatter plots of the actual values vs. the predicted values of Cr(IV) uptake onto lignin by different models have been shown in Fig. 4. In each plot, a precise match between the predicted removal and actual removal is demonstrated by a diagonal straight line. Validation parameters encompassing R^2 , RMSE, MSE, and MAE underpinned the selection of the most accurate model for chromium removal from water. The values of different metrics for various models have been presented in Table 1. It is evident from Fig. 4 that all the models demonstrate a strong alignment with the ideal fit represented by the diagonal straight line. This is also supported by the selected evaluation metrics for this study, indicating that our predictions closely match the actual values. All models exhibited high R^2 values (0.9905 for KNN, followed by 0.9522 for XGBoost, 0.9084 for RF, and 0.8802 for the ANN model). Furthermore, in terms of other metrics (MSE, MAE, and RMSE), the models demonstrated minimal values, indicating minimal error in their predictions, as shown in Table 1. Consequently, the higher R^2 values and lower RMSE, MSE, and MAE values for this study imply that all four models could be applied efficiently for predicting the chromium ions by lignin. Although the performances of all the models were comparable, KNN produced the most accurate predictions, followed by XGBoost, according to the joint scatter plots in Fig. 4 and the results shown in Table 1. These results stipulate that KNN and XGBoost models outperform more competently and accurately to predict the removal efficiency of chromium by the adsorption method, although all the ML models are well acceptable for predicting the adsorption of Cr(VI) onto

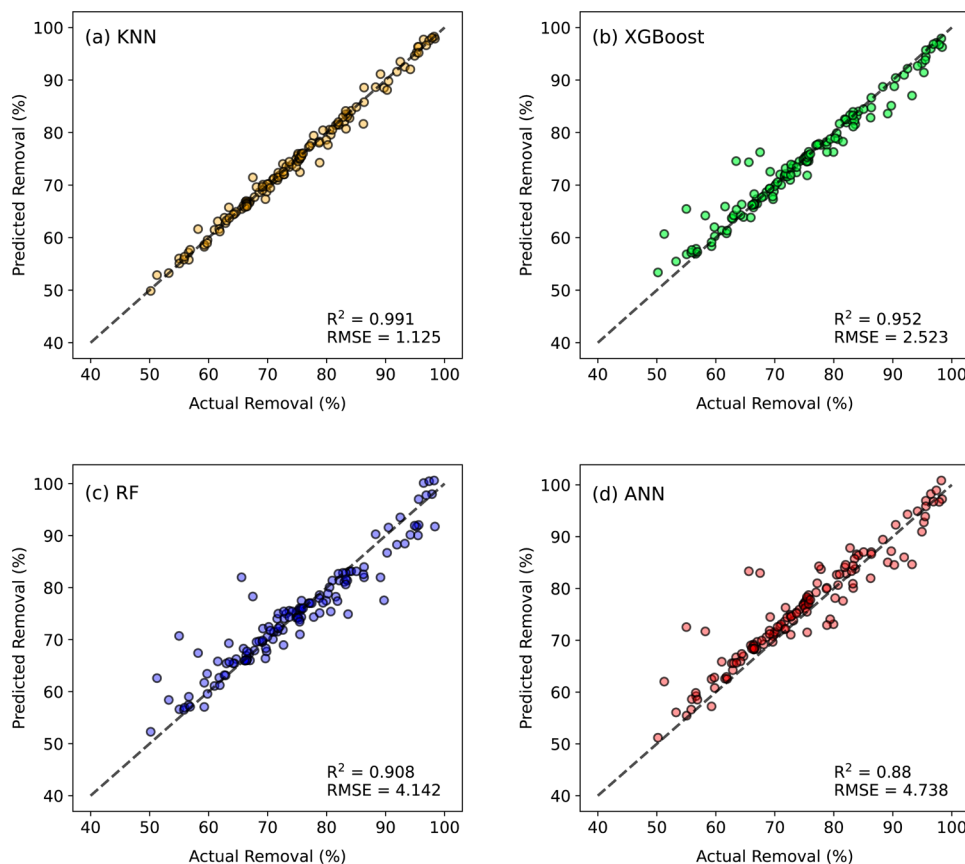


Fig. 4. (a-d) Comparison of removal predicted by different machine learning models and actual removal in the experimental data for the adsorption of Cr(VI) onto lignin.

Table 1. Assessment of predictive performance of applied ML models.

Model	MAE	MSE	RMSE	R ²
KNN	0.7211	1.2655	1.1249	0.9905
XGBoost	1.4001	6.3658	2.5230	0.9522
RF	2.5781	17.1583	4.1422	0.9084
ANN	3.0479	22.4484	4.7379	0.8802

lignin. Herein, KNN and XGBoost models were selected as the best ML algorithms among the four models to develop a chromium adsorption model for further analysis. These results align with the literature on the removal of antibiotics using carbon-based adsorbents (Sigmund et al., 2020).

3.3. Effect of parameters on the adsorption of Cr(VI) by lignin

The well-trained KNN and XGBoost algorithms serve as the reliable predictive models for the removal of chromium by lignin. Thus, these two models are applied to assess the impact of various variables on chromium removal efficiency. The effect of adsorbent dose (experimental black dotted line) and partial dependence plot of a single parameter, like load of adsorbent (red line and blue line obtained from XGBoost and KNN, respectively), has been presented in Fig. 5(a). The removal efficiency demonstrates an upward trend as the lignin dose increases, reaching its peak at 50 mg/L for experimental results, and more than 90% of the dye is removed. However, as the lignin content increases after 50 mg/L, the removal efficiency gradually decreases. This observation suggests the paramount importance of adsorption capacity for eliminating chromium. The observed relationship between removal efficiency and load of lignin can be attributed to the presence of more surface areas and an increased number of active sites for Cr(VI) adsorption. On the contrary, a slight decrease in the removal efficiency with the increase of lignin load over 50 mg/L could be attributed to a

reduction in the number of active adsorbed sites, which is caused by the formation of lignin aggregates through π - π interactions between the aromatic rings of adjacent lignin molecules (Ma et al., 2020; Zhao et al., 2017). The predicted results of KNN and XGBoost models also demonstrated similar trends as the experimental results, except that the maximum removal is found to occur over a range of 40–60 mg/L adsorbent load, and the maximum removal is found to be 78%. The experimental results for removal efficiency as a function of initial concentration of Cr(VI) solution, along with a partial dependence plot for the same input parameter, have been presented in Fig. 5(b). The experimental results closely match the predicted results obtained from the KNN and XGBoost models. The removal efficiency of chromium is found to increase with the initial concentration of Cr(VI) solution, reaching the maximum value at an initial concentration of 50 ppm for experimental results. However, the maximum adsorption is found over the range of 40–60 ppm for both KNN and XGBoost models. As the concentration of Cr(VI) increases, more Cr(VI) ions are available for colliding with the active adsorption sites on the lignin surface, and there is a higher chance for the uptake of Cr(VI) by lignin (Di et al., 2022). Moreover, after a certain concentration (above 50 ppm for experimental and over 60 ppm for predicted results) removal rate is found to decline again gradually with the rise of Cr(VI) concentration. For a definite amount of lignin dose, a certain number of active sorption sites are found. Once Cr(VI) ions saturate the active sites, any rise in metal ion concentration does not produce extra adsorption. This is because the quantity of chromium ions exceeds the number of available active adsorption sites. In addition, as the concentration of metal ions increases, mass transfer resistance increases for the adsorbate to become adsorbed, resulting in a decrease in adsorption. Similar results were also reported for the adsorptive removal of Pb²⁺ ion from aqueous solution by lignin (Liu et al., 2019).

Adsorption duration serves as a pivotal factor indicating the kinetics of adsorption under a specific metal ion concentration. The results show that the slope of removal efficiency is high at the initial

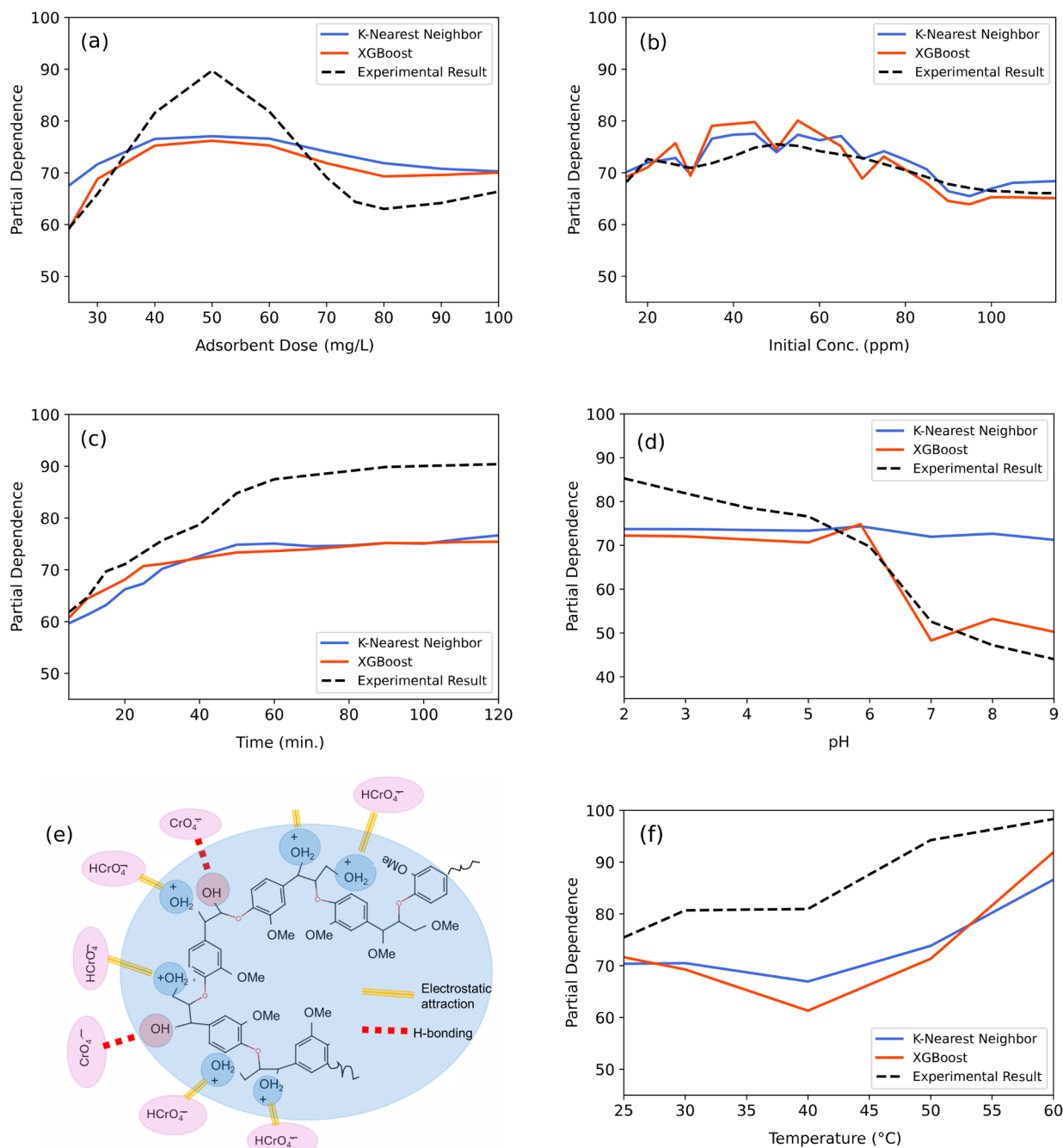


Fig. 5. Comparison between experimental results and partial dependence plots obtained from machine learning models for (a) initial concentration of Cr(VI), (b) lignin dosage, (c) time of adsorption, (d) pH of the medium, (e) adsorption mechanism (f) temperature. Blue and red lines represent the results obtained from KNN and XGBoost models, respectively.

stage of adsorption, and later it reaches a steady value at about 80 min (Fig. 5c). The faster rate of adsorption might be ascribed to the availability of higher active sites at the surface of the adsorbent for the adsorption of chromium. The predicted results exhibit trends similar to the experimental results, but the equilibrium appears to be reached earlier than in the experiment. It is also noticed that more than 90% chromium is removed at equilibrium time (experimental), whereas the predicted results show a maximum removal efficiency of about 70% at equilibrium time.

The surface characteristics of the adsorbent, ionization probability, the charge on the adsorbent surface, and the amount of metal ions in the aqueous medium are strongly governed by pH. The dependency of removal efficiency on pH (experimental) and partial dependence plots for chromium removal by the KNN and XGBoost models have

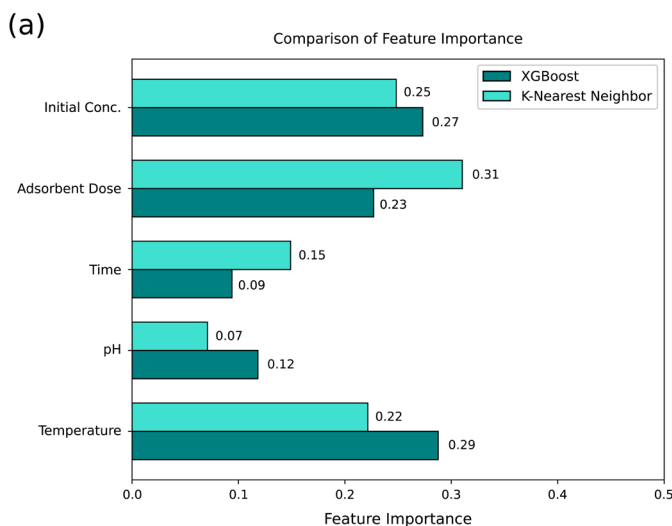
been shown in Fig. 5(d). Higher removal efficiency is observed under acidic conditions and progressively downward with the increase of pH for experimental results. It was observed that uptake of Cr(VI) ions and protonated functional groups of lignin (Demirbaş, 2005). At lower pH (2), the different functional groups of lignin, such as phenolic, hydroxyl, carbonyl groups, etc., are protonated and become positively charged. On the other hand, chromium exists predominantly as HCrO_4^- . As a result, electrostatic interaction between these two oppositely charged particles favors the uptake of Cr(VI) onto lignin (Albadarin et al., 2011). It has been reported that HCrO_4^- ions can easily be diffused toward the lignin surface and get adsorbed (Tazerouti and Amrani, 2009). The removal efficiency is lower at higher values of Tazerouti interfere with HCrO_4^- adsorption by occupying active sites on

the adsorbent. (Albadarin et al., 2011). Moreover, some chromium ions are deposited as chromium hydroxide by the formation of a precipitate at higher pH (Afzaal et al., 2022). It has been reported that conversion of HCrO_4^- to CrO_4^{2-} occurs at higher pH; on the contrary, at higher pH surface charge of lignin is reduced due to deprotonation and hence forms a neutral or a negative surface (Kwak et al., 2016). However, it is observed that more than 40% chromium is removed at higher pH. At higher pH, lignin surface becomes negatively charged and Cr(VI) is reduced to Cr(III) when it comes in contact to lignin via different functional groups (-OH, -O-, C=C, C-O, -OMe), which act as an electron donor, and adsorbs on the lignin surface through H-bonding (Elrayyes et al., 2025; Kwak et al., 2016), as shown in Fig. 5(e). Predicted results of pH also resemble the experimental data. The predicted results of XGBoost demonstrate that removal efficiency is almost steady up to pH 6 and then decreases in a similar way as that of experimental results. The predicted results of KNN demonstrated little deviation from the experimental results, and it is shown that the removal of chromium is not dependent on the change of pH of the suspension. Moreover, the predicted results reveal a little bit lower removal efficiency (72%) than that of the experimental results (85%). The above results suggest the possible mechanism of chromium (VI) ions by lignin and electrostatic interactions, and redox reaction plays the pivotal role for the uptake of Cr(VI) ions by lignin, as represented by Fig. 5(f).

The effect of temperature on the adsorption efficiency has been shown in Fig. 5(f). The figure shows that the percentage of chromium removal initially shows a slightly decreasing trend and then increases sharply as the temperature rises, and a maximum of 98% chromium is removed at 60°C. The decrease in adsorption observed at elevated temperature implies a physical adsorption mechanism. As the temperature rises, the kinetic energy of adsorbate molecules increases, and adsorbate molecules may be released from the active sites of lignin, following a drop in Cr(VI) uptake up to 40°C. When the temperature increases beyond 40°C, the adsorption efficiency is found to increase, which indicates that the process of adsorption is endothermic in nature. The high temperature might alter the adsorbent, its active sites, and activity, and augment the chemical interaction between Cr(VI) and lignin. Furthermore, high temperature might enhance the diffusion rate of chromium from the bulk to the surface of lignin, which results in an increase in Cr(VI) adsorption. The predicted results also demonstrate similar behavior as experimental results, but the percentage of removal is found to be lower than experimental results.

3.4 Correlation analysis

Fig. 6 displays the relative importance of various input parameters based on two best-performing models (KNN and XGBoost). It has been found from Fig. 6(a) that the removal efficacy of Cr(VI) ions has a strong correlation with adsorbent dose, temperature, and initial concentration, but has a weak correlation with time and pH of the medium. These results



suggest that the common vital independent parameters are adsorbent (lignin) dose, initial concentration of chromium, and temperature. For the KNN model, the adsorbent dose ranked highest among these independent variables (31%), followed by initial concentration (25%) and temperature (22%). For the XGBoost model, the most influential parameters are temperature (29%), initial concentration (27%), and adsorbent dose (23%), respectively. This result reveals that the adsorption capacity of chromium by lignin is primarily affected by the lignin dose, initial concentration of chromium ions, and temperature. Similar findings have been reported for dye adsorption by agricultural waste using several machine learning algorithms in previous studies (Moosavi et al., 2021). Moreover, the removal efficiency of chromium ions is found to be positively correlated with the initial concentration of chromium ions, lignin dose, adsorption time, temperature, and pH of the medium, as shown by the Pearson correlation matrix in Fig. 6(b). Initial concentrations of chromium have a positive correlation with adsorbent dose because as the dose of adsorbent and initial concentration of chromium ions increase, more fresh adsorbed sites become available for adsorption of more chromium ions. Again, the lignin dose negatively correlates with the time. This result indicates that once all adsorption sites are occupied and equilibrium is reached, no significant adsorption occurs beyond this point due to a lack of available sites after a definite time interval.

3.5 Double factor analysis

The two-factor PDP analysis was utilized to evaluate the synergistic relationship between adsorption conditions. Figs. 7(a and b) for XGBoost and KNN, respectively) represents the combined effect of two variables (initial concentration of Cr(VI) and lignin dose) on the removal efficiency of chromium. It is found that the dependence of removal efficiency is higher at lower concentrations of chromium ions and lower doses of adsorbent. The maximum uptake was observed at chromium ion concentration of 30–50 ppm and an adsorbent dose of 40–60 mg/L for both models, followed by a gradual decline at higher concentration and dose. The overall maximum removal efficiency was 75%, which is lower than the experimental results mentioned earlier. With increasing chromium concentration and adsorbent dose, more metal ions and more active adsorption sites become available, leading to improved efficiency (Kabir et al., 2025; Miah et al., 2017). However, at higher concentrations, mass transfer is restricted (due to a reduced effective diffusion coefficient of ions (Bilbao et al., 2016; Miah et al., 2016). Additionally, some lignin molecules (at a higher dosage) might aggregate due to π - π interactions between adjacent aromatic layers, reducing the number of available active sites for adsorption (Ma et al., 2020).

The combined effect of two variables, the initial concentration of chromium ions and temperature, has been presented in Figs. 7(c and d) for XGBoost and KNN, respectively. It is noticed that the temperature

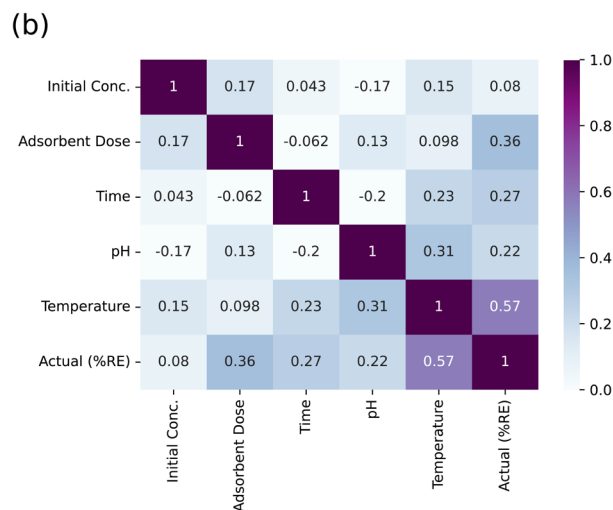


Fig. 6. (a) Relative importance of input features based on KNN and XGBoost models, and (b) Pearson correlation matrix between any two variables and removal efficiency.

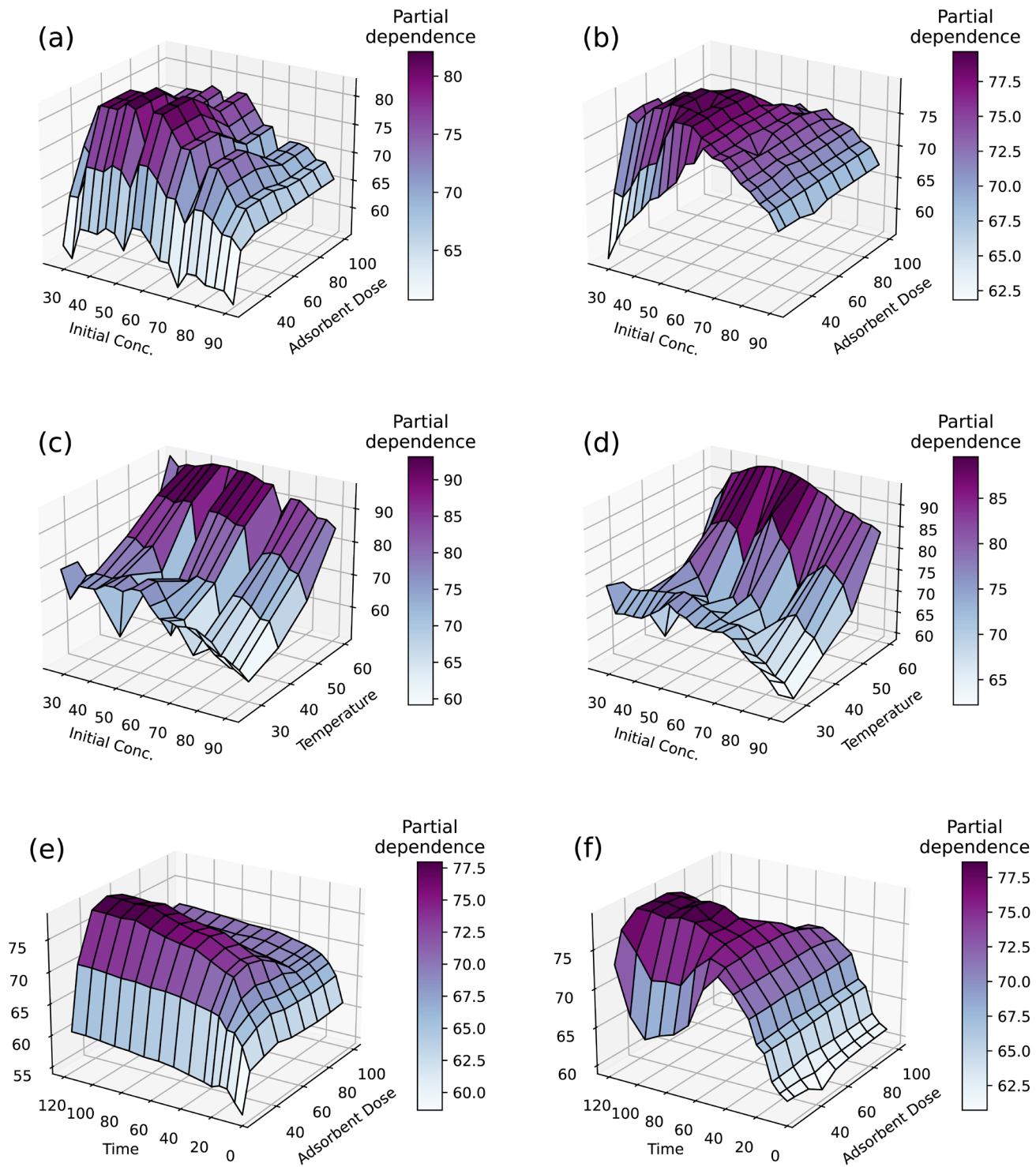


Fig. 7. Two-factor partial dependence (a and b) effect of initial concentration of chromium ion vs. dose of adsorbent, (c and d) effect of initial concentration vs. temperature, (e and f) effect of contact time vs adsorbent dose according to XGBoost and KNN model, respectively, for the removal of chromium by lignin.

had a comparatively greater impact on the removal efficiency than the initial concentration of chromium ions for both models. The results show that removal efficiency is better at higher temperatures and moderate initial concentrations of chromium ions. In contrast, it has been shown that the percentage of removal decreases at lower temperatures, both for lower concentrations and higher concentrations of metal ions, likely owing to the combined influence of these factors. It is noteworthy that the removal efficiency exhibits an increasing trend with an initial increase in concentration, followed by minimal

fluctuation, and thereafter a declining trend with further increases in concentration. The maximum removal efficiency is found within the concentration range of 40–50 ppm. However, an increasing trend of removal efficiency is observed with the rise of temperature, and the maximum efficiency is found at 60°C for both KNN and XGBoost models. At elevated temperatures, mass transfer kinetics are enhanced because of the increase in kinetic energy of adsorbates, and more adsorption sites are activated through physical and chemical interactions, resulting in higher removal efficiency (Bilbao et al., 2016).

The mutual interaction of two variables, adsorbent dose and adsorption time, has been presented in Figs. 7(e and f) for XGBoost and KNN, respectively. The combined effect of contact time and adsorbent dose manifests in the gradual increase in removal efficiency with contact time for both models. An initial increase of removal efficiency followed by a decreasing trend with adsorbent dose is found for both models, and the maximum removal efficiency is observed over the time frame of 80–120 min and adsorbent dose of 40–60 mg/L. An abundant number of functional groups (alcoholic –OH, phenolic –OH, –CO–, –COOH, methoxy group, and sulfonic groups) of lignin are available to interact with chromium ions. Thus, higher removal is observed at moderate adsorbent load, but at higher load, some adsorbent molecules might form aggregates or coagulate, resulting in a decline in removal efficiency (Kabir et al., 2025).

3.6 Adsorption isotherm analysis

Adsorption isotherms were studied by using chromium solutions of 3 mg/L to 40 mg/L, and the resulting data were applied to the Langmuir isotherm and the Freundlich isotherm models, represented by Eqs. (7) and (8), respectively.

$$Q_e = \frac{Q_{max} K_L C_e}{1 + K_L C_e} \tag{7}$$

$$Q_e = K_F C_e^{\frac{1}{n}} \tag{8}$$

Where C_e is the concentration (mg/L) of Cr(VI) at equilibrium, Q_e is the amount of chromium (mg/g) at equilibrium, q_{max} is the adsorption

capacity (mg/g) of lignin at monolayer coverage, K_L is the Langmuir adsorption constant, K_F is the Freundlich adsorption constant ($\text{mg}^{1-1/n} \text{L}^{-1/n} \text{g}^{-1}$), n is a constant related to adsorption intensity.

Fig. 8(a) shows that the correlation coefficient for the adsorption of chromium by lignin is 0.987 for the Langmuir model and 0.930 for the Freundlich model. These results indicate that experimental data of the adsorption of chromium by lignin is more well-fitted to the Langmuir model than the Freundlich model. Fitting the experimental data to the Langmuir isotherm provided that the amount of chromium for monolayer coverage, i.e., the maximum adsorption capacity of chromium by lignin, was 97.06 mg/g. Fitting of experimental data to the Freundlich isotherm provided the value of $1/n = 0.887$, indicating that the adsorption of chromium onto the surface of lignin is favorable (Sume et al., 2024).

3.7 Adsorption kinetic analysis

To elucidate the adsorption kinetics, several experiments were conducted at various time spans, and the resulting data were applied to the pseudo-first-order and second-order kinetic models, as described by Eqs. (9) and (10).

$$Q_t = Q_e (1 - e^{-k_1 t}) \tag{9}$$

$$Q_t = \frac{Q_e^2 K_2 t}{1 + K_2 Q_e t} \tag{10}$$

Where t is the time of adsorption, Q_t is the adsorption capacity (mg/g) at time t , Q_e is the equilibrium adsorption capacity (mg/L),

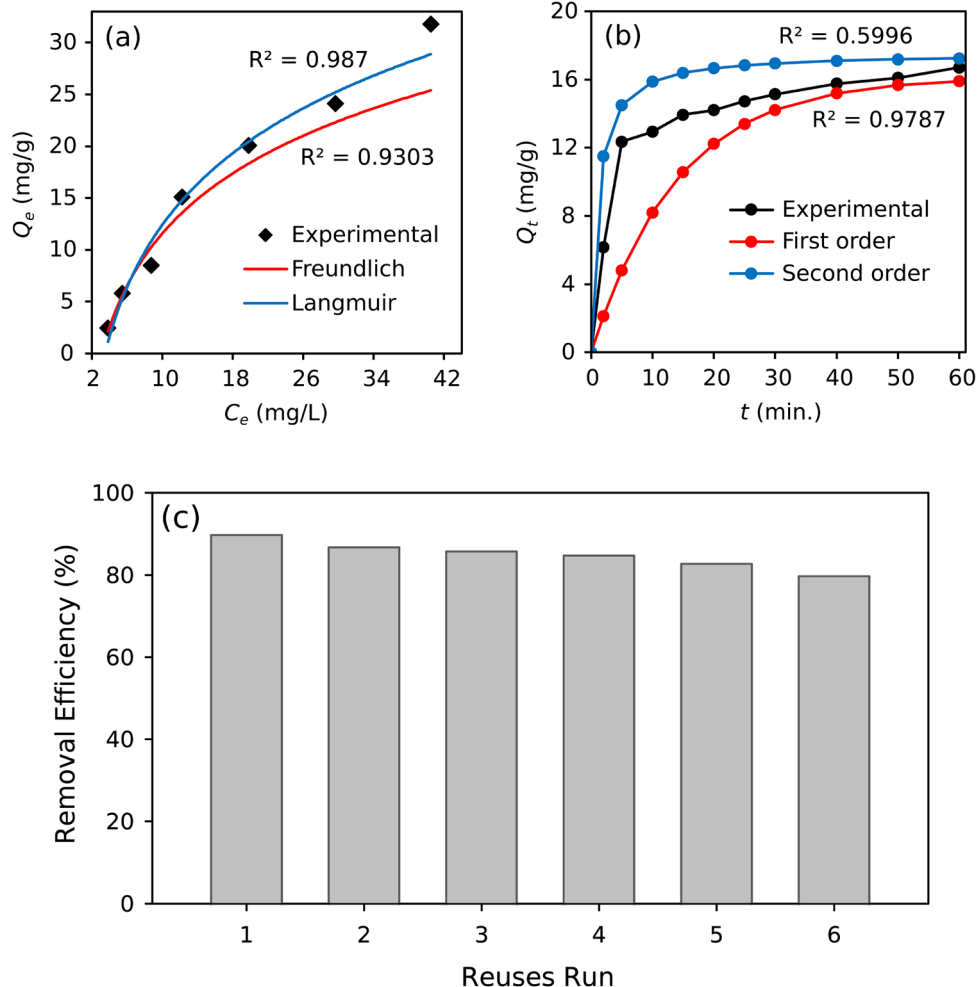


Fig. 8. Study of (a) adsorption isotherm, (b) adsorption kinetics for the removal of Cr(VI) by lignin, and (c) recycling test of lignin.

Table 2.

Comparative study of lignin and other biosorbents for the removal of Cr(VI) from aqueous solution.

Adsorbent	Adsorption capacity (mg/g)	References
Lignin-based resin	74.29	(Liang <i>et al.</i> , 2013)
Poplar lignin	93.78	(Du <i>et al.</i> , 2020)
Sugarcane bagasse lignin	28.04	(Nguyen-Thi <i>et al.</i> , 2024)
Biochar of lignin-rich kiwifruit branches	143.64	(Bian and Shao, 2024)
Cucumis melo activated carbon	54.28	(El Kassimi <i>et al.</i> , 2024)
Cow waste	66.4	(Elrayyes <i>et al.</i> , 2025)
Jute sticks lignin	97.06	In this work

and K_1 (min^{-1}) and K_2 ($\text{g}/\text{mg min}$) are the adsorption rate constants for pseudo-first-order and second-order models, respectively.

The experimental data for the adsorption of chromium by lignin were fitted to the two kinetic models, and the fitted graphs have been presented in Fig. 8(b). It has been found that the correlation coefficient for the pseudo-first-order kinetic model is 0.978, and the pseudo-second-order kinetic model is 0.899. This indicates that the pseudo-first-order kinetic model is more appropriate to describe the adsorption behavior of chromium by lignin (Kayes *et al.*, 2016; Sume *et al.*, 2024).

3.8 Recycling test and comparison with lignin-based adsorbent

To evaluate the regeneration efficiency of lignin, after completion of adsorption, Cr(VI) loaded lignin was immersed in 0.1M NaOH solution and stirred continuously for 120 min to achieve complete desorption of chromium. The adsorption–desorption process was repeated for up to six cycles, and the regeneration efficiency of lignin has been shown in Fig. 8(c). From the figure, it is observed that chromium removal efficiency declines gradually, reaching about 80% after six consecutive cycles. It was reported that lignin molecules dissolved to some extent at higher pH. During regeneration of lignin with NaOH treatment, the pH of the solution approaches 13, which contributes to lignin dissolution and the reduction of Cr(VI) (Albadarin *et al.*, 2011). Although the regeneration efficiency of lignin decreases over repeated cycles, it still demonstrates a considerable potential (~80%) for eliminating Cr(VI) ions from the water environment. This suggests that lignin serves as an efficient, cost-effective, and widely abundant biosorbent for eliminating heavy metals from wastewater.

The maximum adsorption capacities of different bio-based adsorbents have been presented in Table 2. Lignin demonstrates a comparable adsorption capacity for the removal of Cr(VI) ions from aqueous solution, establishing itself as a strong contender for contaminant removal. Considering prime factors such as the low cost, wide availability of raw materials, and the ability to regenerate and reuse with minimal performance loss, strengthens its practical value, making it well-suited for large-scale applications. Even though its capacity is slightly lower compared to some modified biochar/composite adsorbents, it still performs competitively against high-end adsorbents like functionalized activated carbons.

4. Conclusions

This study investigates the optimization and modeling of Cr(VI) adsorption onto lignin. The batch adsorption experiments were conducted by varying different parameters, including concentration, dose, pH, time, and temperature. The optimum conditions for the adsorption experiment were determined, and maximum Adsorption capacities of lignin were found to be 97.06 mg g^{-1} at pH 2, and a dose of 50 mg L^{-1} . Adsorption data and correlation coefficient analysis suggested that the adsorption process followed the Langmuir isotherm ($R^2 = 0.987$) and the pseudo-first-order kinetics model ($R^2 = 0.978$). The experimental results were then fed into the ML algorithms to determine the influence of individual and double variables on the adsorption process, and to identify the most influential variables in the adsorption of chromium

ions by lignin. Different ML models, including RF, XGBoost, ANN, and KNN, were employed to predict the impact of various physicochemical variables on the adsorption of Cr(VI) by lignin. Four performance metrics, such as MAE, MSE, RMSE, and R^2 , were used to evaluate the performance of each ML algorithm. The Pearson correlation matrix showed that removal efficiency was positively correlated with initial concentration, lignin dose, adsorption time, temperature, and pH of the medium. Predicted results further demonstrated that among the different physicochemical parameters, adsorbent dose was the most influential parameter, followed by temperature and initial concentration. The performance analysis revealed that, among the different ML models, XGBoost and KNN predicted the actual removal efficiency with the highest accuracy and precision. The ML models, developed directly from experimental data, provided reliable predictability for removing chromium ions from aqueous solutions under variable environmental conditions. It is expected that this endeavor will reduce the cost and repeat experimental procedures for the design and application of any method for removing contaminants from wastewater.

CRedit authorship contribution statement

Nadim Ahmed: Conceptualization, methodology, software, validation, data curation, writing - original draft, writing - review & editing, visualization. **Abdullah Al Rakib:** Conceptualization, resources, data curation, investigation, validation, writing - original draft. **Md. Shahabuddin:** Conceptualization, formal analysis, writing - review & editing, supervision. **Mohammad Shahid Ullah:** Conceptualization, formal analysis, writing - review & editing, supervision. **Md. Nurnobi Rashed:** Conceptualization, formal analysis, writing - review & editing, supervision. **Md Jalil Miah:** Conceptualization, resources, formal analysis, writing - original draft, writing - review & editing, project administration, supervision

Declaration of competing interest

The authors declare that they have no competing financial interests or personal relationships that could have influenced the work presented in this paper.

Data availability

The datasets used or analyzed during the current study are available from the corresponding author on reasonable request.

Declaration of generative AI and AI-assisted technologies in the writing process

The authors confirm that there was no use of artificial intelligence (AI)-assisted technology for assisting in the writing or editing of the manuscript and no images were manipulated using AI.

Supplementary data

Supplementary material to this article can be found online at https://dx.doi.org/10.25259/JKSUS_1395_2025.

References

- Afzaal, M., Hameed, S., Abbasi, N.A., Liaqat, I., Rasheed, R., Khan, A.A.manatA., Manan, H.abdul, 2022. Removal of Cr (III) from wastewater by using raw and chemically modified sawdust and corn husk. *Water Pract Technol* 17, 1937-1958. <https://doi.org/10.2166/wpt.2022.093>
- Albadarin, A.B., Al-Muhtaseb, A.'ah., Al-laqtah, N.A., Walker, G.M., Allen, S.J., Ahmad, M.N.M., 2011. Biosorption of toxic chromium from aqueous phase by lignin: Mechanism, effect of other metal ions and salts. *Chem Eng J* 169, 20-30. <https://doi.org/10.1016/j.cej.2011.02.044>
- Altmann, A., Tološi, L., Sander, O., Lengauer, T., 2010. Permutation importance: A corrected feature importance measure. *Bioinformatics* 26, 1340-1347. <https://doi.org/10.1093/bioinformatics/btq134>
- Apicella, A., Donnarumma, F., Isgro, F., Prevete, R., 2021. A survey on modern trainable activation functions. *Neural Netw* 138, 14-32. <https://doi.org/10.1016/j.neunet.2021.01.026>

- Benesty, J., Chen, J., Huang, Y., & Cohen, I., 2009. Pearson Correlation Coefficient. *Springer Topics in Signal Processing*, 2, 14. https://doi.org/10.1007/978-3-642-00296-0_5
- Bergstra J., & Bengio Y., 2012. Random search for hyper-parameter optimization. *J. Mech Learn Res.* 13, 281-305. <https://doi.org/10.5555/2188385.2188395>
- Bilbao, L., Ortueta, M., Mijangos, F., 2016. Effect of concentration and temperature on mass transfer in metal ion exchange. *Ind Eng Chem Res* 55, 7287-7295. <https://doi.org/10.1021/acs.iecr.6b00398>
- Breiman, L., 2001. Random forests. *Machine Learning* 45, 5-32. <https://doi.org/10.1023/a:1010933404324>
- Chen, T., Guestrin, C., 2016. XGBoost. KDD '16: The 22nd ACM SIGKDD international conference on knowledge discovery and data mining San Francisco California USA, pp. 785-794. <https://doi.org/10.1145/2939672.2939785>
- Choudhary, V., Patel, M., Pittman, C.U., Mohan, D., 2020. Batch and continuous fixed-bed lead removal using Himalayan pine needle biochar: Isotherm and kinetic studies. *ACS Omega* 5, 16366-16378. <https://doi.org/10.1021/acsomega.0c00216>
- Demirbaş, A., 2005. Adsorption of Cr(III) and Cr(VI) Ions from aqueous solutions on to modified lignin. *Energy Sources* 27, 1449-1455. <https://doi.org/10.1080/009083190523352>
- DesMarais, T.L., Costa, M., 2019. Mechanisms of chromium-induced toxicity. *Curr Opin Toxicol* 14, 1-7. <https://doi.org/10.1016/j.cotox.2019.05.003>
- Di, J., Ruan, Z., Zhang, S., Dong, Y., Fu, S., Li, H., Jiang, G., 2022. Adsorption behaviors and mechanisms of Cu²⁺, Zn²⁺ and Pb²⁺ by magnetically modified lignite. *Sci Rep* 12, 1394. <https://doi.org/10.1038/s41598-022-05453-y>
- Dobbelaere, M.R., Plehiers, P.P., Van de Vijver, R., Stevens, C.V., Van Geem, K.M., 2021. Machine learning in chemical engineering: strengths, weaknesses, opportunities, and threats. *Eng* 7, 1201-1211. <https://doi.org/10.1016/j.eng.2021.03.019>
- Dutta, S.K., Amin, M.K., Ahmed, J., Elias, M., Mahiuddin, M., 2022. Removal of toxic methyl orange by a cost-free and eco-friendly adsorbent: Mechanism, phytotoxicity, thermodynamics, and kinetics. *South African J Chem Eng* 40, 195-208. <https://doi.org/10.1016/j.sajce.2022.03.006>
- El-Rayyes, A., Arogundade, I., Ogundiran, A.A., Hefnawy, M., Ofudje, E.A., El Gamal, A., Albedair, L.A., Alsuhaibani, A.M., 2025. Hot water-treated cow waste use as an efficient adsorbent for cresol red dye and chromium VI removal from aqueous solutions. *Biores* 20, 3252-3285. <https://doi.org/10.15376/biores.20.2.3252-3285>
- Friedman, J. H. (2001). Greedy function approximation: A gradient boosting machine. 29, 11891232. <https://doi.org/10.1214/AOS/1013203451>
- Han, X., Wong, Y.S., Wong, M.H., Tam, N.F., 2007. Biosorption and bioreduction of Cr(VI) by a microalgal isolate, *Chlorella miniata*. *J Hazard Mater* 146, 65-72. <https://doi.org/10.1016/j.jhazmat.2006.11.053>
- Jain, A.K., Jianchang Mao, Mohiuddin, K.M., 1996. Artificial neural networks: A tutorial. *Computer* 29, 31-44. <https://doi.org/10.1109/2.485891>
- Kabir, M.H., Miah, M.J., Mohiuddin, A.K., Hossain, M.S., Upoma, B.P., Shaikh, M.A.A., Pabel, M.Y., Mojumder, F., Mahmud, R., Tanvir, N.I., Yasmin, S., 2025. Highly Effective Removal of Moxifloxacin from Aqueous Solutions Using Graphene Oxide Functionalized with Sodium Dodecyl Sulfate. *ACS Sustainable Resour Manage* 2, 256-266. <https://doi.org/10.1021/acssusresmg.4c00296>
- Kayes, N., Miah, J., Obaidullah, M., Hossain, A., Hossain, M., 2016. Immobilization of ZnO suspension on glass substrate to remove filtration during the removal of remazol red r from aqueous solution. *JAC* 12, 4127-4133. <https://doi.org/10.24297/jac.v12i6.6990>
- Keiluweit, M., Nico, P.S., Johnson, M.G., Kleber, M., 2010. Dynamic molecular structure of plant biomass-derived black carbon (biochar). *Environ Sci Technol* 44, 1247-1253. <https://doi.org/10.1021/es9031419>
- Kramer, O., 2013. Dimensionality Reduction with Unsupervised Nearest Neighbors. *Intelligent Systems Reference Library*, 51, 13-23. <https://doi.org/10.1007/978-3-642-38652-7>
- Kumar, V., Dwivedi, S.K., 2021. A review on accessible techniques for removal of hexavalent Chromium and divalent Nickel from industrial wastewater: Recent research and future outlook. *J Cleaner Prod* 295, 126229. <https://doi.org/10.1016/j.jclepro.2021.126229>
- Kwak, H.W., Shin, M., Yun, H., Lee, K.H., 2016. Preparation of silk sericin/lignin blend beads for the removal of hexavalent chromium ions. *Int J Mol Sci* 17, 1466. <https://doi.org/10.3390/ijms17091466>
- Li, F., Zimmerman, A.R., Hu, X., Gao, B., 2020. Removal of aqueous Cr(VI) by Zn- and Al-modified hydrochar. *Chemosphere* 260, 127610. <https://doi.org/10.1016/j.chemosphere.2020.127610>
- Li, Y., Chang, J., Kong, C., Bao, W., 2022. Recent progress of machine learning in flow modeling and active flow control. *Chin J Aeronautics* 35, 14-44. <https://doi.org/10.1016/j.cja.2021.07.027>
- Liu, C., Li, Y., Hou, Y., 2019. Preparation of a novel lignin nanosphere adsorbent for enhancing adsorption of lead. *Molecules* 24, 2704. <https://doi.org/10.3390/molecules24152704>
- Ma, M., Dai, L., Xu, J., Liu, Z., Ni, Y., 2020. A simple and effective approach to fabricate lignin nanoparticles with tunable sizes based on lignin fractionation. *Green Chem* 22, 2011-2017. <https://doi.org/10.1039/d0gc00377h>
- Mamudur, K., Kattamuri, M.R., 2020. Application of boosting-based ensemble learning method for the prediction of compression index. *J Inst Eng India Ser A* 101, 409-419. <https://doi.org/10.1007/s40030-020-00443-7>
- Md Salim, R., Asik, J., Sarjadi, M.S., 2021. Chemical functional groups of extractives, cellulose and lignin extracted from native *Leucaena leucocephala* bark. *Wood Sci Technol* 55, 295-313. <https://doi.org/10.1007/s00226-020-01258-2>
- Miah, M.J., Aziz, M.T., Kayes, M.N., Obaidullah, M., Hossain, M.M., 2017. Decolorization of remazol black B in aqueous suspension of TiO₂. *Br J Environ Sci* 5, 51-70.
- Miah, M.J., Kayes, M.N., Obaidullah, M., Hossain, M.M., 2016. Photodegradation efficiency of prepared and commercial ZnO to remove textile dye from aqueous solution. *J Adv Chem Sci* 337-340.
- Mohamad Ibrahim, M.N., Zakaria, N., Sipaut, C.S., Sulaiman, O., Hashim, R., 2011. Chemical and thermal properties of lignins from oil palm biomass as a substitute for phenol in a phenol formaldehyde resin production. *Carbohydr Polym* 86, 112-119. <https://doi.org/10.1016/j.carbpol.2011.04.018>
- Molnar, C., Casalicchio, G., Bischl, B., 2020. Interpretable Machine Learning A Brief History, State-of-the-Art and Challenges. *Communications in Computer and Information Science*, 1323, 417431. https://doi.org/10.1007/978-3-030-65965-3_28
- Moosavi, S., Manta, O., El-Badry, Y.A., Hussein, E.E., El-Bahy, Z.M., Mohd Fawzi, N., FarizaB., Urbonavičius, J., Moosavi, S.M.H., 2021. A study on machine learning methods' Application for dye adsorption prediction onto agricultural waste activated carbon. *Nanomaterials* 11, 2734. <https://doi.org/10.3390/nano11102734>
- Moriassi, D.N., Arnold, J.G., Van Liew, M.W., Bingner, R.L., Harmel, R.D., Veith, T.L., 2007. Model evaluation guidelines for systematic quantification of accuracy in watershed simulations. *Trans ASABE* 50, 885-900.
- Nguyen-Thi, N.Y., Nguyen, C.Q., Le Dang, Q., De Tran, Q., Do-Thi, T.N., Vu Thanh, L.H., 2024. Extracting lignin from sugarcane bagasse for methylene blue and hexavalent chromium adsorption in textile wastewater: A facile, green, and sustainable approach. *RSC Adv* 14, 4533-4542. <https://doi.org/10.1039/d3ra08007b>
- Nickens, K.P., Patierno, S.R., Ceryak, S., 2010. Chromium genotoxicity: A double-edged sword. *Chem Biol Interact* 188, 276-288. <https://doi.org/10.1016/j.cbi.2010.04.018>
- Othmani, A., Magdoul, S., Senthil Kumar, P., Kapoor, A., Chellam, P.V., Gökküs, Ö., 2022. Agricultural waste materials for adsorptive removal of phenols, chromium (VI) and cadmium (II) from wastewater: A review. *Environ Res* 204, 111916. <https://doi.org/10.1016/j.envres.2021.111916>
- Papaevangelou, V., Bakalakou, K.A., Tsilini, K.I., Akrotos, C.S., 2023. Testing zeolite and palygorskite as a potential medium for ammonium recovery and brewery wastewater treatment. *Water* 15, 4069. <https://doi.org/10.3390/w15234069>
- Pereira, S.C., Oliveira, P.F., Oliveira, S.R., Pereira, M.L., Alves, M.G., 2021. Impact of environmental and lifestyle use of chromium on male fertility: Focus on antioxidant activity and oxidative stress. *Antioxidants (Basel)* 10, 1365. <https://doi.org/10.3390/antiox10091365>
- Prabu, D., Kumar, P.S., Rathi, B.S., Sathish, S., Anand, K.V., Kumar, J.A., Mohammed, O.B., Silambarasan, P., 2022. Feasibility of magnetic nano adsorbent impregnated with activated carbon from animal bone waste: Application for the chromium (VI) removal. *Environ Res* 203, 111813. <https://doi.org/10.1016/j.envres.2021.111813>
- ProbstPhilipp, BoulesteixAnne-Laure, & BischlBernrd., 2019. Tunability. *The Journal of Machine Learning Research* 20, 1934-1965. <https://doi.org/10.48550/arXiv.1802.09596>
- Refaeilzadeh, P., Tang, L., & Liu, H., 2009. Cross-Validation. *Encyclopedia of Database Systems*, 532538. https://doi.org/10.1007/978-0-387-39940-9_565
- Shahmansouri, A.A., Akbarzadeh Bengar, H., Jahani, E., 2019. Predicting compressive strength and electrical resistivity of eco-friendly concrete containing natural zeolite via GEP algorithm. *Constr Build Mater* 229, 116883. <https://doi.org/10.1016/j.conbuildmat.2019.116883>
- Sigmund, G., Gharasoo, M., Hüffer, T., Hofmann, T., 2020. Deep learning neural network approach for predicting the sorption of ionizable and polar organic pollutants to a wide range of carbonaceous materials. *Environ Sci Technol* 54, 4583-4591. <https://doi.org/10.1021/acs.est.9b06287>
- Singh, N., Gupta, S.K., 2016. Adsorption of heavy metals: a review. *Int. J. Innov. Res. Sci. Eng. Technol.* 5, 22672281. <https://doi.org/10.15680/IJRSET.2016.050146>
- Sume, S.A., Tabassum, M., Ali, M.K., Suhag, M.H., Kayes, M.N., 2024. Preparation and characterization of acid and base modified fish scales of laebo rohita and their application as an adsorbent. *J Eng Adv* 5, 88-93. <https://doi.org/10.38032/jea.2024.03.004>
- Sun, H., Brocato, J., Costa, M., 2015. Oral chromium exposure and toxicity. *Curr Environ Health Rep* 2, 295-303. <https://doi.org/10.1007/s40572-015-0054-z>
- Taoufik, N., Boumya, W., Achak, M., Chennouk, H., Dewil, R., Barka, N., 2022. The state of art on the prediction of efficiency and modeling of the processes of pollutants removal based on machine learning. *Sci Total Environ* 807, 150554. <https://doi.org/10.1016/j.scitotenv.2021.150554>
- Tazerouti, N., Amrani, M., 2009. Chromium (VI) Adsorption on Activated Lignin. *Chemical Product and Process Modeling*, 4, 1-19. <https://doi.org/10.2202/1934-2659.1339>
- Troiano, J.M., Jordan, D.S., Hull, C.J., Geiger, F.M., 2013. Interaction of Cr(III) and Cr(VI) with hematite studied by second harmonic generation. *J Phys Chem C* 117, 5164-5171. <https://doi.org/10.1021/jp3122819>
- Wu, Y., Li, Y., Jiang, Z., Xu, Z., Yang, M., Ding, J., Zhang, C., 2023. Machine learning prediction of phosphate adsorption on six different metal-containing adsorbents. *ACS EST Eng* 3, 1135-1146. <https://doi.org/10.1021/acsesteng.3c00001>
- Zafar, M., Aggarwal, A., Rene, E.R., Barbusiński, K., Mahanty, B., Behera, S.K., 2022. Data-driven machine learning intelligent tools for predicting chromium removal in an adsorption system. *Processes* 10, 447. <https://doi.org/10.3390/pr10030447>
- Zhang, W., Ashraf, W.M., Senadheera, S.S., Alessi, D.S., Tack, F.M.G., Ok, Y.S., 2023. Machine learning based prediction and experimental validation of arsenite and arsenate sorption on biochars. *Sci Total Environ* 904, 166678. <https://doi.org/10.1016/j.scitotenv.2023.166678>
- Zhao, W., Xiao, L.P., Song, G., Sun, R.C., He, L., Singh, S., Simmons, B.A., Cheng, G., 2017. From lignin subunits to aggregates: Insights into lignin solubilization. *Green Chem* 19, 3272-3281. <https://doi.org/10.1039/c7gc00944e>
- Zhu, X., Wan, Z., Tsang, D. C. W., He, M., Hou, D., Su, Z., Shang, J., 2021. Machine learning for the selection of carbon-based materials for tetracycline and sulfamethoxazole adsorption. *Chemical Engineering Journal*, 406, 126782-126788. <https://doi.org/10.1016/j.cej.2020.126782>
- Zhu, X., Wang, X., Ok, Y.S., 2019. The application of machine learning methods for prediction of metal sorption onto biochars. *Journal of Hazardous Materials*, 378, 120727-120733. <https://doi.org/10.1016/J.JHAZMAT.2019.06.004>